



Valley focusing effect in a rippled graphene superlattice

M. Pudlak *Institute of Experimental Physics, 04001 Kosice, Slovakia*R. G. Nazmitdinov **Bogoliubov Laboratory of Theoretical Physics, Joint Institute for Nuclear Research, 141980 Dubna, Moscow region, Russia
and Dubna State University, 141982 Dubna, Moscow region, Russia*

(Received 28 February 2024; revised 10 April 2024; accepted 17 April 2024; published 2 May 2024)

Graphene corrugations affect hybridization of π and σ orbitals of carbon atoms in graphene based systems. It can as well break differently the symmetry of the electron transfer integrals for different strip boundaries. Using these facts, we found that the momentum distribution of electrons in ballistically propagating beam can be selective without external electric and/or magnetic fields in the graphene strip under experimentally feasible periodic potential. Such a potential is created by means of the superlattice that consists of periodically repeated graphene elements (flat and rippled junction) with different hybridization of carbon orbits, produced by variation of the graphene surface curvature. As a result it gives rise to the valley dependent focusing effects that can be controlled by alteration of the number of superlattice elements.

DOI: [10.1103/PhysRevB.109.205402](https://doi.org/10.1103/PhysRevB.109.205402)

I. INTRODUCTION

The exceptionally high charge carrier mobility in graphene has generated enormous experimental and theoretical activity, with various potential applications in nanotechnology in mind (see textbooks [1,2]). The remarkable graphene properties have been explained as a consequence of linear energy dispersion of the gapless low-energy excitations, provided by graphene crystal structure that consists of two equivalent carbon sublattices. Consequently, one can introduce graphene quasiparticles with different pseudospin quantum numbers associated with the corresponding sublattices. It is notable that this linear energy dispersion in the low-energy spectrum of graphene is similar to the Dirac-Weyl equation for massless neutrino [3].

It was shown in [4] that the conservation of the pseudospin forbids strictly charged carrier backscattering in a graphene monolayer with electrostatic potential scattering that mimics the n - p junction. The barrier always remains perfectly transparent for the normal incidence of electrons, while the transmission decreases for other angles. By virtue of this fact, electron focusing analogous to optical effects that occur in negative refractive index material is predicted [5]. It is noteworthy to mention that the above discussed results are based on assumption of use of external electrical or magnetic accessories to control the focusing of electron flow.

We recall, however, that graphene sheets are not perfectly flat, and ripples are considered as most natural sources that might be used to control the electron mobility as well. A number of proposals have been suggested in support of this idea. It was predicted in the tight-binding approximation

that a corrugation (ripple) could create in graphene electron scattering, caused by the change in nearest-neighbor hopping parameters by the curvature [6,7]. Further on, it was found that electrons in opposite valleys can be perfectly transmitted or totally reflected in the presence of strain [8]. In Ref. [9] it was shown how inhomogeneous strains can be used to create wave guides for valley polarized transport of Dirac fermions in graphene.

Note that the lattice deformation changes the distance between ions, p_z orbital orientation, and is leading to shift of the on-site energies of p_z orbitals. This affects the effective Dirac equation that could simulate the low energy electron states as a result of a deformation-induced gauge field [10]. Moreover, the lattice deformation changes the relative orientation of the orbitals of the corrugated graphene sheet, leading to the hybridizations of the π and σ bonds (see details in the Appendix). The π orbital dependence on the surface curvature means that the local chemical potential varies with the curvature. In fact, the hybridization leads to inhomogeneous charge distribution, and acts as potential barriers for electrons leading to their localization [11]. This effect becomes important once it would be possible to create a graphene system with controlled variation of the surface curvature. In fact, the DFT and molecular dynamics simulations predict that the graphene sheet can be stretched up to about 20%–30% without being damaged [12]. The amplitude and the orientation of the unidirectional ripples can be controlled with the aid of the applied strain [13]. Further, it was shown that by using the hydrogenation it is possible to induce periodic ripples with various thermal conductivity [14].

The discussed above theoretical ideas are supported, indeed, by a few experimental techniques that demonstrate evidently a spatial variation in graphene sheets nowadays. The strain effect can be achieved by putting the material on substrate that is microstructured [15] or mechanically

*rashid@theor.jinr.ru

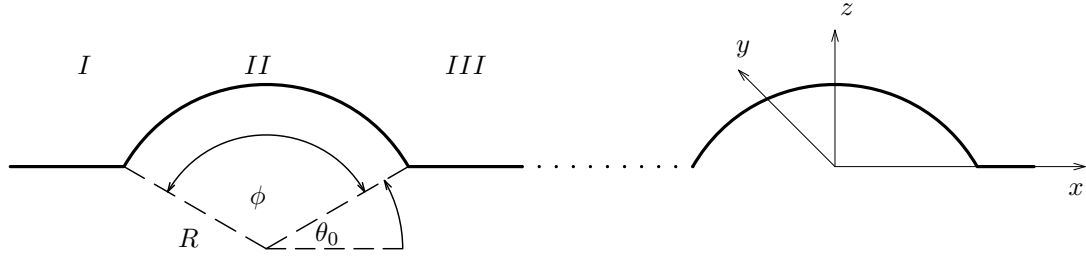


FIG. 1. The corrugated graphene structure. The flat graphene pieces are located in region (I), $-\infty < x < -R \cos \theta_0$, $-\infty < y < \infty$; and region (III), $R \cos \theta_0 < x < \infty$, $-\infty < y < \infty$. In region (II), $-R \cos \theta_0 < x < R \cos \theta_0$ and $-\infty < y < \infty$, we consider a ripple (a curved surface in a form of arc of a circle). The ripples are ordered in the x direction with the symmetry y axis.

deformed [16]. Ripples can be formed by means of the electrostatic manipulation without any change of doping [17]. Periodically rippled graphene can be fabricated by the epitaxial technique (e.g., [18]). In this case, in contrast to free-standing graphene, a strong modification of the electronic structure of graphene is observed, that gives rise to localized phonon [19] and plasmon [20] modes. Periodic nanoripples can be created as well by means of the chemical vapor deposition [21]. It is found that ripples or wrinkles act as potential barriers for charged carriers leading to their localization [22], in agreement with the theoretical estimations [11].

One of the main aims of the present paper is to demonstrate that strain effects could provide the ability of the valleytronics to manipulate and detect the valley degree of freedom of the ballistic electron transport. To this aim we employ the model of rippled graphene superlattice discussed in [23,24]. In the present paper we extended this model by considering the dependence of the hopping integrals between π orbitals in zigzag and armchair graphene surface curvatures following the approach developed by Ando [25]. We recall that typical transition lengths for n - p junctions are less than 100 nm (e.g., [26]), which allows to employ a ballistic transport model for the study of physics n - p junction devices [27]. To demonstrate the effect of valleytronics, various authors introduced either electrical/magnetic fields or additional potentials to simulate strain effects (see for a review [28]). We will show that the effective potential determined by the variation of the local curvature of the graphene sheet provides an additional design degree of freedom for both fundamental studies and graphene-based electronic devices.

II. SCATTERING MODEL

We suppose that incident ballistic electrons move from the left planar graphene piece to the right planar piece passing through N elements of the superlattice. The unit element of the superlattice is composed of one ripple and one planar piece. The graphene strip (the superlattice) is terminated in the x direction by zigzag or armchair boundaries, while it infinitely long in the y direction. Each element represents a single junction described below.

A. Eigenvalue problem

The corrugated graphene structure is modeled by a curved surface in a form of an arc of a circle connected from the

left-hand and the right-hand sides to two flat graphene sheets (see Fig. 1). Hereafter, we consider a wide enough graphene sheet $W \gg M$, where W and M are, respectively, the width along the y axis and the length along x axis of the graphene sheet. It means that we keep the translational invariance along the y axis and neglect the edge effects.

To analyze our junction, we take into account (i) the variation of the hybridization of the carbon atom orbitals with a surface curvature of a graphene sheet (see the Appendix); and (ii) the modification of the electron transfer integrals, caused by the variation of the surface curvature. The variation of the hybridization can be described by an effective electric potential $\varepsilon(x)$. The modification of the electron transfer integrals can be calculated as a shift of a vector potential $\Delta \hat{k}$ in the matrix Hamiltonian in the effective mass approximation. In order to find these modifications we extended the approach, developed by Ando (see discussion in Ref. [25]), and derived the corresponding Hamiltonian (the details will be published elsewhere). Thus, in the effective mass approximation the eigenvalue problem for the envelope function can be written in the following form:

$$\begin{pmatrix} \varepsilon(x) & D_\tau \\ D_{-\tau} & \varepsilon(x) \end{pmatrix} \begin{pmatrix} F_A \\ F_B \end{pmatrix} = E \begin{pmatrix} F_A \\ F_B \end{pmatrix}, \quad (1)$$

$$D_\tau = \gamma[(\hat{k}_x + \Delta k_x) - i\tau(\hat{k}_y + \Delta k_y)], \quad (2)$$

where $\tau = +$ corresponds to the K point, while $\tau = -$ corresponds to the K' point. The two components of the wavefunction refer to the two sublattices of carbon atoms. The additional spin degeneracy of the excitations are not important in our consideration.

As it is shown in the Appendix, the dependence of energy ε_π on the local surface curvature can be expressed in the form

$$\varepsilon_\pi = \varepsilon_{2p} + \alpha \left(\frac{a}{R}\right)^2. \quad (3)$$

Here $\varepsilon_{2p} = \langle p_z | H | p_z \rangle$ is the $|p_z\rangle$ orbital energy of the carbon atom, R is the ripple radius, and $\alpha = -0.58$ eV. Thus, the energy difference between the π orbitals in the curved and flat graphene is

$$\varepsilon = \varepsilon_{2p} - \varepsilon_\pi = \Delta\varepsilon = |\alpha| \left(\frac{a}{R}\right)^2 \approx 0.58 \left(\frac{a}{R}\right)^2 \text{ eV}. \quad (4)$$

This difference can be considered as a contribution of the effective electric field produced by the curvature dependence of the hybridization. In the case of the flat graphene

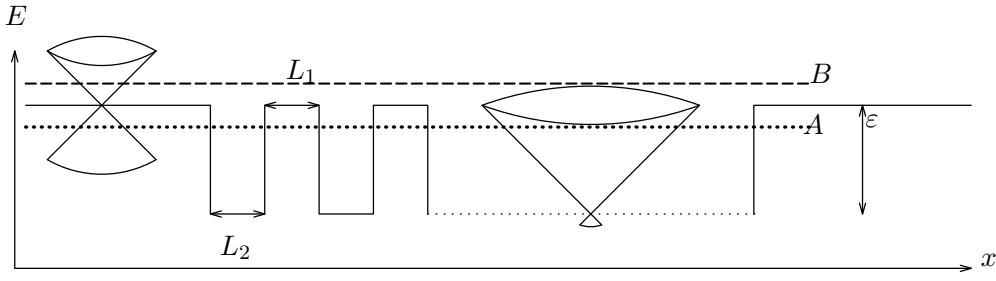


FIG. 2. A schematic illustration of the scattering process in the superlattice composed of N elements. Each element contains the flat region of the length L_1 connected to the ripple of the length L_2 . The energy ε is brought about by the curvature dependence of the hybridization effect (see text). For a separate undoped flat graphene sheet (\mathcal{F}), the Fermi energy lies exactly at the Dirac point ε_{2p} (indicated by a solid line that crosses the Dirac point, the left side). A similar picture takes place for a separate curved graphene piece (\mathcal{C}), where the position of the Fermi energy ε_π , indicated by the dotted line on the right side. For the hybrid system that consists of $\mathcal{F} + \mathcal{C}$ pieces, there are two cases with the electron incident energies indicated by the lines A and B.

$R \rightarrow \infty$ and, consequently, $\varepsilon(x) = \varepsilon_{2p}$. The difference between ε_π (curved region) and ε_{2p} (flat region) is important when the systems with different surface curvature are coupled. Hereafter, for the sake of simplicity we assume that $\varepsilon_\pi = 0$.

In the flat regions (I and III), the eigenstate of Eq. (1) has the following form:

$$F(x, y) = e^{ik_x x} e^{ik_y y} \frac{1}{\sqrt{2}} \begin{pmatrix} s e^{-i\varphi} \\ 1 \end{pmatrix}, \quad s = \pm 1, \quad (5)$$

and the eigenenergy is

$$E = \varepsilon + s\gamma \sqrt{k_x^2 + k_y^2}, \quad (6)$$

where $s = +1(-1)$ is associated with the conduction (valence) band. Here

$$e^{-i\varphi} = \frac{k_x - ik_y}{\sqrt{k_x^2 + k_y^2}}. \quad (7)$$

The eigenfunction and eigenenergy in region II (a ripple) are obtained in the following forms:

$$F(x, y) = e^{ik_x x} e^{ik_y y} \frac{1}{\sqrt{2}} \begin{pmatrix} s e^{-i\chi} \\ 1 \end{pmatrix}, \quad (8)$$

$$E = s\gamma \sqrt{(\kappa_x + \Delta\kappa_x)^2 + (k_y + \Delta k_y)^2}. \quad (9)$$

Here

$$e^{-i\chi} = \frac{(\kappa_x + \Delta\kappa_x) - i(k_y + \Delta k_y)}{\sqrt{(\kappa_x + \Delta\kappa_x)^2 + (k_y + \Delta k_y)^2}}. \quad (10)$$

The vector field $\vec{\Delta k}$ depends on the graphene surface curvature. The concrete form of this field will be used to investigate the transport properties of a corrugated graphene with zigzag and armchair boundaries.

We assume that the flat segment has the length L_1 , while the a ripple has the length $L_2 = R\phi$, see Figs. 1 and 2. We consider the scattering at the interface introduced by different hybridizations in the flat and the curved graphene regions. The interface is assumed to be smooth on the length scale of a graphene unit cell (an inverse Brillouin momentum $2\pi/K$).

Consequently, it does not induce the intervalley ($K \rightarrow K'$) scattering.

B. Transport phenomena

1. Single junction

Before we analyze the ballistic transport through the superlattice \mathcal{S} we have to consider the transmission of electrons, traveling with energy E through the hybrid subsystem $\mathcal{F} + \mathcal{C}$ (the unit element), at two most typical cases: above and below the effective potential ε (see Fig. 2). In the both cases we have to match the corresponding wave functions in the flat and curved graphene pieces.

In the first flat (\mathcal{F}) sector of the \mathcal{S} region [$X_L \leq x < X_L + L_1$, $|y| < W$] we consider the wave function in the form

$$\Psi(x, y) = \frac{e^{ik_y y}}{\sqrt{2}} \left\{ e^{ik_x x} \begin{pmatrix} e^{-i\varphi} \\ 1 \end{pmatrix} + r e^{-ik_x x} \begin{pmatrix} -e^{i\varphi} \\ 1 \end{pmatrix} \right\}, \quad (11)$$

and for the first rippled (\mathcal{C}) sector of the \mathcal{S} region [$X_L + L_1 \leq x < X_L + L_1 + L_2$, $|y| < W$] we define the wave function in the form

$$\Psi(x, y) = \frac{e^{ik_y y}}{\sqrt{2}} \left\{ \alpha_1 e^{i\kappa_x x} \begin{pmatrix} e^{-i\chi} \\ 1 \end{pmatrix} + \beta_1 e^{-i\kappa_x x} \begin{pmatrix} -e^{i\chi} \\ 1 \end{pmatrix} \right\}, \quad (12)$$

and so on. For the last flat region [$X_L + N(L_1 + L_2) \leq x < M$, $|y| < W$] we have

$$\Psi(x, y) = \frac{e^{ik_y y}}{\sqrt{2}} t e^{ik_x x} \begin{pmatrix} e^{-i\varphi} \\ 1 \end{pmatrix}. \quad (13)$$

The unknown coefficients α_i, β_i can be obtained from the continuity conditions on the boundaries.

Let us consider the specific features of the transmission, related to the incident electron energy E with regard to the effective potential ε .

(i) $E > \varepsilon$.

In this case we have the following condition for the incident electron energy E (denoted as a line B in Fig. 2):

$$E = \varepsilon + \gamma \sqrt{k_x^2 + k_y^2} = \gamma \sqrt{(\kappa_x + \Delta\kappa_x)^2 + (k_y + \Delta k_y)^2}. \quad (14)$$

For this particular case we obtain for transmission coefficients

$$T_{11} = e^{ik_x L_1} [\cos \kappa_x L_2 - i \sin \kappa_x L_2 f^{(-)}], \quad (15)$$

$$T_{11} = T_{22}^*, \quad (16)$$

where

$$f^{(\pm)} = \frac{1 \pm \sin \varphi \sin \chi}{\cos \varphi \cos \chi}, \quad (17)$$

and

$$T_{21} = e^{-i\varphi} e^{ik_x L_1} \sin \kappa_x L_2 \frac{\sin \chi - \sin \varphi}{\cos \varphi \cos \chi}, \quad (18)$$

$$T_{21} = T_{12}^*. \quad (19)$$

Based on the above relations, we have the following useful equation

$$\frac{T_{11} + T_{22}}{2} = a_1 - a_2 f^{(-)}, \quad (20)$$

$$a_1 = \cos k_x L_1 \cos \kappa_x L_2, \quad (21)$$

$$a_2 = \sin k_x L_1 \sin \kappa_x L_2. \quad (22)$$

The valley dependence relations between quantities k_y , k_x , κ_x are defined by Eq. (14).

(ii) $0 < E < \varepsilon$.

In this case we have the following condition for the incident electron energy E (denoted as a line A in Fig. 2):

$$E = \varepsilon - \gamma \sqrt{k_x^2 + k_y^2} = \gamma \sqrt{(\kappa_x + \Delta k_x)^2 + (k_y + \Delta k_y)^2}. \quad (23)$$

For transmission coefficients we obtain the following results:

$$T_{11} = e^{-ik_x L_1} [\cos \kappa_x L_2 + i \sin \kappa_x L_2 f^{(+)}], \quad (24)$$

$$T_{21} = e^{-i\varphi} e^{ik_x L_1} \sin \kappa_x L_2 \frac{\sin \chi + \sin \varphi}{\cos \varphi \cos \chi}. \quad (25)$$

The same relations, Eqs. (16) and (19), are valid as well, which yield another useful equation:

$$\frac{T_{11} + T_{22}}{2} = a_1 + a_2 f^{(+)}. \quad (26)$$

Here, the relations between k_y , k_x , κ_x are defined by Eq. (23).

2. Superlattice

Using the continuity conditions on boundaries, we arrive to the equations for the transmission coefficient t through the block of N ripples and the corresponding reflection coefficient r :

$$\begin{pmatrix} 1 \\ r \end{pmatrix} = \begin{pmatrix} T_{11} & T_{12} \\ T_{21} & T_{22} \end{pmatrix}^N = \begin{pmatrix} N_{11} & N_{12} \\ N_{21} & N_{22} \end{pmatrix} \begin{pmatrix} t \\ 0 \end{pmatrix}. \quad (27)$$

These equations yield the obvious relations:

$$t = 1/N_{11}; \quad r = N_{21} t. \quad (28)$$

With the aid of Eqs. (15)–(19), (24), and (25) it is ready to show that

$$\det(T) = 1. \quad (29)$$

We recall that the T matrix is subject to the condition

$$\begin{pmatrix} T_{11} & T_{12} \\ T_{21} & T_{22} \end{pmatrix} \begin{pmatrix} a \\ b \end{pmatrix} = \lambda \begin{pmatrix} a \\ b \end{pmatrix}. \quad (30)$$

With the aid of Eqs. (29) and (30), we obtain the eigenvalues

$$\lambda_{1,2} = \beta \pm \sqrt{\beta^2 - 1}, \quad \beta = (T_{11} + T_{22})/2. \quad (31)$$

The transformation U (that diagonalizes the matrix T)

$$U = \begin{pmatrix} a_1 & a_2 \\ b_1 & b_2 \end{pmatrix} \Rightarrow U^{-1} T U = \begin{pmatrix} \lambda_1 & 0 \\ 0 & \lambda_2 \end{pmatrix} \quad (32)$$

yields, in virtue of Eqs. (27) and (32), the following relation:

$$U \begin{pmatrix} \lambda_1^N & 0 \\ 0 & \lambda_2^N \end{pmatrix} U^{-1} = \begin{pmatrix} N_{11} & N_{12} \\ N_{21} & N_{22} \end{pmatrix}. \quad (33)$$

By means of the standard procedure it is ready to obtain the matrices U and U^{-1} ($U U^{-1} = 1$). As a result, taking into account that $\lambda_1 \lambda_2 = 1$, we obtain the following definitions:

$$N_{11} = \frac{T_{11}(\lambda_1^N - \lambda_2^N) + \lambda_2^{N-1} - \lambda_1^{N-1}}{\lambda_1 - \lambda_2} = N_{22}^*, \quad (34)$$

$$N_{12} = T_{12} \frac{\lambda_2^N - \lambda_1^N}{\lambda_2 - \lambda_1} = N_{21}^*. \quad (35)$$

Evidently, the relation (27) between the matrices T and N , and Eq. (29) yield the fulfillment of the following condition:

$$\det(N) = \begin{vmatrix} N_{11} & N_{12} \\ N_{21} & N_{22} \end{vmatrix} = |N_{11}|^2 - |N_{21}|^2 = 1. \quad (36)$$

This secures that the condition $|r|^2 + |t|^2 = 1$ is fulfilled, taking into account the definitions Eq. (28). As a result, by means of Eqs. (28), (36), and the definition (35), we obtain the following expression for the total transmission probability through N elements of the superlattice:

$$\begin{aligned} T_N = |t|^2 &= \frac{1}{|N_{11}|^2} = \frac{1}{1 + |N_{21}|^2} \\ &= \frac{1}{1 + |T_{12}|^2 \left(\frac{\lambda_2^N - \lambda_1^N}{\lambda_2 - \lambda_1} \right)^2}. \end{aligned} \quad (37)$$

Evidently, the transmission probability (37) is a function of the incident electron energy E that determines the motion along the superlattice [i.e., the wave numbers k_x and k_y ; see Eqs. (6) and (9)]. It is convenient to determine the transmission probability as a function of the wave number k_y which together with the wave number $k_F = |E - \varepsilon|/\gamma$ determines details of electron transport. With the aid of the transmission probability, the conductance is given by the Landauer formula:

$$G_N = 4 \frac{e^2}{h} \int_{-k_F}^{k_F} T_N(k_y) \frac{dk_y}{2\pi/W} = 4 \frac{e^2}{h} \frac{k_F W}{\pi} I_N. \quad (38)$$

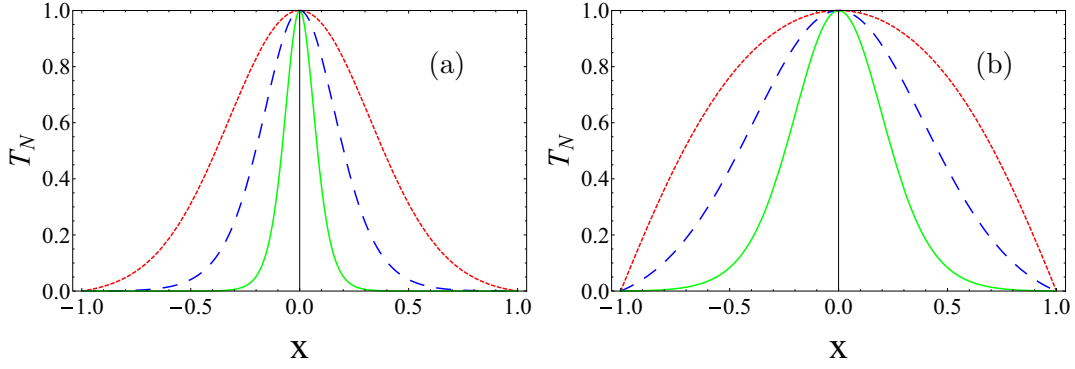


FIG. 3. Zigzag surface. Transmission probabilities T_N as a function of $x = k_y/k_F$ for $N = 10$ elements (dotted line); $N = 20$ elements (dashed line); $N = 50$ elements (solid line). The energy of the incoming electrons is $E = \varepsilon/2$, $L_1 = 10a$, $a \simeq 2.46 \text{ \AA}$, $\phi = \pi$; (a) $R = 8 \text{ \AA}$; (b) $R = 18 \text{ \AA}$.

Here, the integral I_N , defined by the expression

$$I_N = \frac{1}{2} \int_{-1}^1 T_N(u) du, \quad u = \frac{k_y}{k_F}, \quad (39)$$

characterizes the efficiency of the selection specific electron trajectories entering into the considered system.

For the perfect transmission, i.e., for $T(k_y) = 1$, the conductance

$$G_o = 4 \frac{e^2}{h} \int_{-k_F}^{k_F} \frac{dk_y}{2\pi/W} = 4 \frac{e^2}{\pi h} k_F W \quad (40)$$

is the natural unit, since $G_N = G_o I_N$. For the discussion below we introduce the following terms:

$$G_N^+ = \frac{G_o}{2} \int_0^1 T_N(u) du, \quad G_N^- = \frac{G_o}{2} \int_{-1}^0 T_N(u) du. \quad (41)$$

III. DISCUSSION

Let us analyze common and distinctive properties of the transport through the superlattice with zigzag and armchair graphene surface curvatures. In order to illuminate the effect of the dependence on two interfaces, we have to calculate the shift in the origin of $k_{x,y}$ by $\Delta k_{x,y}$, produced by terms of the order of $(a/R)^2$. In our analysis we follow the arguments discussed by Ando (see Sec. 5 in [25]). The most interesting case is the transport phenomena at the incident electron energy $0 \leq E \leq \varepsilon$ (see Fig. 2, line A), which we study below in detail.

(i) Zigzag surface.

In the effective mass approximation for the zigzag interface, we obtain

$$\Delta k_x = \mp \frac{a}{4\sqrt{3}R^2} \left(1 - \frac{3}{8} \frac{\gamma'}{\gamma} \right), \quad (42)$$

$$\Delta k_y = 0, \quad (43)$$

where the upper sign corresponds to the K point, while the lower sign to the K' point. The parameter $\gamma = \sqrt{3}\gamma_0 a/2 = -\sqrt{3}V_{pp}^\pi a/2$, $\gamma' = \sqrt{3}(V_{pp}^\sigma - V_{pp}^\pi)a/2$, where V_{pp}^π and V_{pp}^σ are the hopping integrals for π and σ orbitals, a is the length of the primitive translation vector. We recall that in our model it is assumed that $V_{pp}^\pi \approx -3 \text{ eV}$ and $V_{pp}^\sigma \approx 5 \text{ eV}$. Therefore, we have $\gamma'/\gamma \approx 8/3$, i.e., $\Delta k_x \approx 0$. Thus, in the

case of zigzag interface, the shifts are negligibly small, i.e., $\Delta k_x \approx 0$ and $\Delta k_y = 0$. It seems that in this case the symmetry between K and K' is conserved.

In order to trace the dependence of the transmission probability on the incident angle of electrons, we calculate numerically Eq. (37) as a function k_y (see Fig. 3). It is noteworthy that the superlattice leads to the selective transmission of electrons. For a small number of N elements in the \mathcal{S} subsystem the transmission probability is nonzero for a wide range of values of k_y (see results for $N = 10, 20$). However, the larger the number of N elements in the superlattice, the stronger the selectivity effect for ballistic electrons. Our system focuses the electronic flow, selecting the transmission of those trajectories that are close to the normal incidence. In fact, for a large enough number of N elements of the superlattice, the selection does not depend on the incident direction of an electron flow at all. Indeed, at $N \gg 1$, only for the direction perpendicular to the surface of the \mathcal{S} subsystem, there is almost the ideal transmission, while for the other angles ($k_y \neq 0$) there is only reflection. Note, however, that the increase of the ripple radius decreases the selectivity effect [see Fig. 3(b)].

The selective electrons transmission across the interface created by N units is demonstrated in Fig. 4, where the dependence of G_N/G_o on the length of the flat region L_1 is depicted. The electron conductivity G_N across the interface with N units is much smaller in comparison to G_o for enough large N at a relatively small value of the flat region $L_1 \leq 10a$ in the superlattice at the small value of the ripple radius $R = 8 \text{ \AA}$. With the increase of the flat region $L_1 \geq 18a$ the conductivity tends to the limit manifested for a small number of ripples, simultaneously losing the selective properties. For a large ripple radius $R = 18 \text{ \AA}$ the selectivity effect and the conductivity decrease with the increase of the flat region L_1 [see Fig. 4(b)]. Thus, there is an optimal set of parameters, such as the ripple radius R , the flat region length L_1 , and the number of elements of the superlattice, which provide the most efficient focusing effect. We return to this point below.

(ii) Armchair surface.

In the effective mass approximation for the armchair interface, we obtain

$$\Delta k_x = 0, \quad (44)$$

$$\Delta k_y = \mp \frac{1}{4\sqrt{3}a} \left(\frac{a}{R} \right)^2 \left(\frac{5}{8} \frac{\gamma'}{\gamma} - 1 \right) \sim \mp \frac{1}{6\sqrt{3}a} \left(\frac{a}{R} \right)^2. \quad (45)$$

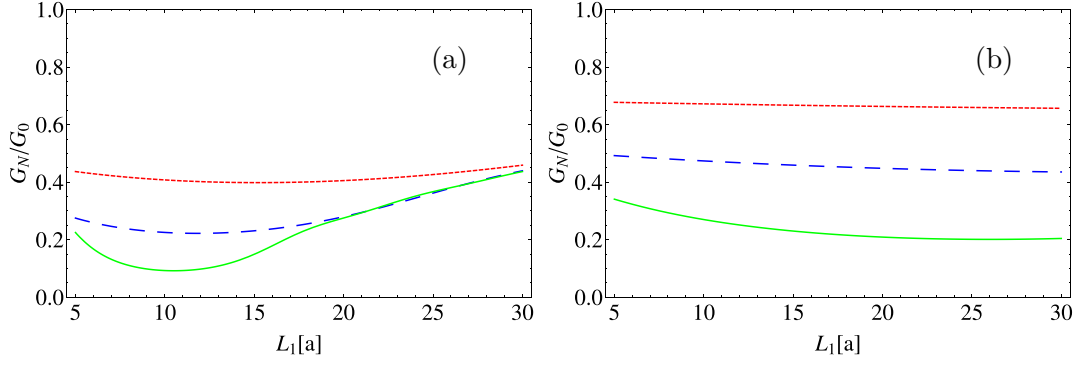


FIG. 4. The conductivity G_N/G_0 as a function of the length L_1 of the flat region in a units. Similar parameters are used as for Fig. 3.

In many ways, the transport properties of this system are similar to those of the zigzag surface (see Figs. 3 and 4). The basic difference consists in the asymmetry of the focusing effects in K and K' valleys (see Fig. 5). It was speculated in Ref. [29] that the vector fields arising from strain might be utilized to impose a valley-dependent filtering in a corrugated graphene sheet. Indeed, our results demonstrate evidently that the replacement $\varphi \rightarrow -\varphi$ leads to a mirror image of the conductivity behavior in the other valley ($K \leftrightarrow K'$). It is notable to mention that the electron conductivity is very similar to the one studied above. Indeed, the conductivity decreases with increase of ripple radius (see Fig. 6). However, for the zigzag edge termination there is a decrease of the contribution G_N^\pm/G_0 around the position $x = 0$. In contrast, with a total decrease of the conductivity in the system with the armchair edge termination there is a prevailing of the G_N^+/G_0 contribution over the G_N^-/G_0 contribution around the position of the supercollimation angle (see Figs. 5 and 6) with the increase of the number of N elements. We return to this point below in detail.

To illuminate the basic features of the transport in the superlattice, let us compare the selectivity effects of the latter case with that produced by the smooth step [4,30]. We recall

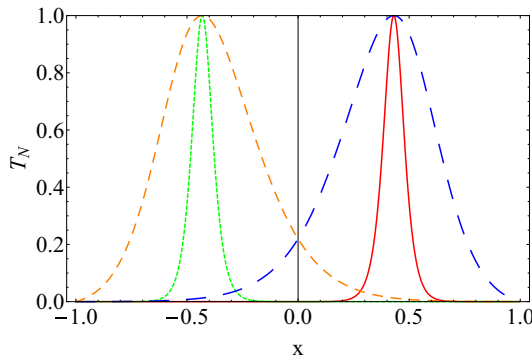


FIG. 5. Armchair surface. Transmission probabilities T_N as a function of $x = k_y/k_F$ for (i) $N = 15$ elements (valley K , long dashed line), (valley K' , short dashed line); and (ii) $N = 70$ elements (valley K , solid line), (valley K' , dotted line). Filtering in φ space, induced by N elements of the superlattice, results in valley focusing effect. The action of a φ filter allows for electrons in valley K to be transmitted freely, while blocking them in valley K' at the same value of the angle φ . The energy of the incoming electrons is $E = \varepsilon/2$, $L_1 = 10a$, $a \simeq 2.46 \text{ \AA}$, $\phi = \pi$, and $R = 8 \text{ \AA}$.

that the estimation for the smooth step (which produces the focusing) yields the value

$$G_{sm} = 2 \frac{e^2}{\pi h} W \sqrt{\frac{k_F}{l}} = \frac{G_0}{2\sqrt{k_F \ell}}, \quad (46)$$

that describes the conductivity at the condition $k_F \ell \gg 1$ (ℓ is the step length). In order to achieve the smooth step effect, the corrugations with gradually increasing curvature can be used in our case. This conditions leads to the inequality

$$G_{sm} > G_N \Rightarrow \sqrt{2\pi \ell / \lambda_F} \times I_N < 1/2. \quad (47)$$

If we hold fixed the condition $\ell = N(L_1 + L_2)$, this inequality determines the number of elements N and their length $L_1 + L_2$ at the same length ℓ for the smooth potential and the superlattice. Thus, by appropriate choice of the product $N(L_1 + L_2)$, one can always use the advantage of electron flow focusing through the superlattice, where a number of elements can be controlled externally. Moreover, one can additionally use the fine tuning of the ripple radius and change carrier charge densities on different sides of our hybrid system.

For completeness we present the results for transmission probabilities at $E > \varepsilon$ for different surfaces (see Fig. 7). Again, we observe the conservation of symmetry between K and K' valleys in a graphene sheet with a zigzag surface, while it is broken in that with an armchair surface. We found that the number of the ripples has a slight influence on the electron transmission.

Depending on the energy of the incident electron beam it is possible to determine analytically the angle of the supercollimation in the case of the zigzag and armchair edge terminations. Evidently, this angle is subject to the condition $T_N = 1 \Rightarrow |T_{12}|^2 \equiv |T_{21}|^2 = 0$ [see Eq. (37)], which holds for the incident electron energy $E > \varepsilon$ and $E < \varepsilon$. Let us consider each case in detail.

(i) $E > \varepsilon$: In this case the condition $|T_{12}|^2 = 0 \Rightarrow \sin \varphi = \sin \chi$ [see Eq. (18)]. Since the energy of incoming electrons in the flat graphene piece $E = \varepsilon + \gamma \sqrt{k_x^2 + k_y^2}$, we have [see also Eq. (7)]

$$\sin \varphi = \frac{k_y}{(E - \varepsilon)/\gamma}. \quad (48)$$

Taking into account the definition of energy of transmitted electrons in the curved graphene piece $E = \gamma \sqrt{(\kappa_x + \Delta \kappa_x)^2 + (k_y + \Delta k_y)^2}$, we have [see also

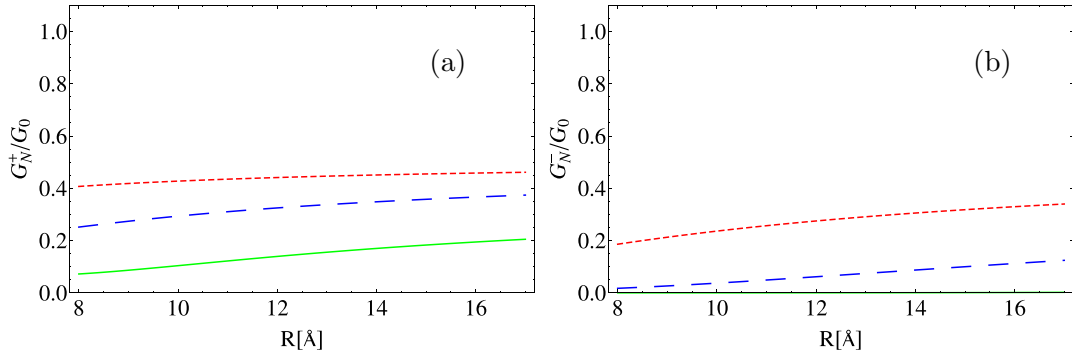


FIG. 6. The conductivity G_N^\pm/G_0 as a function of the ripple radius R in a units for $N = 5$ elements (dotted line); $N = 15$ elements (dashed line); and $N = 60$ (solid line). The incident electron energy is $E = \varepsilon/2$, $L_1 = 10a$, and $\phi = \pi$, armchair surface. The results are given for valley K .

Eq. (10)]

$$\sin \chi = \frac{k_y + \Delta k_y}{E/\gamma}. \quad (49)$$

As a result, we obtain

$$\sin \chi = \sin \varphi \Rightarrow x = \frac{k_y}{k_F} = \frac{\gamma \Delta k_y}{\varepsilon}, \quad (50)$$

where $k_F = (E - \varepsilon)\gamma$, and Δk_y is determined by Eq. (45).

(ii) $E < \varepsilon$. In this case the condition $|T_{12}|^2 = 0 \Rightarrow \sin \varphi = -\sin \chi$ [see Eq. (25)]. Since in the flat graphene piece the energy of incoming electrons (moving in the valence band, see Fig. 2) is $E = \varepsilon - \gamma\sqrt{k_x^2 + k_y^2}$ [see also Eq. (23)], we have

$$\sin \varphi = \frac{k_y}{(\varepsilon - E)/\gamma}. \quad (51)$$

Taking into account Eq. (49), we obtain

$$\sin \varphi = -\sin \chi \Rightarrow x = \frac{k_y}{k_F} = -\frac{\gamma \Delta k_y}{\varepsilon}. \quad (52)$$

Thus, we obtain the definition of the supercollimation angle that is determined by the contribution ε produced by a curvature dependence hybridization, and by a magnitude of the vector field $\Delta \vec{k}$ brought about by a graphene surface curvature. In particular, at the incident electron energy $E < \varepsilon$,

we obtain for valley K ,

$$\begin{aligned} \sin \varphi &= -\left(\frac{\gamma \tau |\Delta k_y|}{\varepsilon}\right) \\ &= \left[\frac{\sqrt{3}}{2} a \gamma_0 \frac{1}{6\sqrt{3}a} \left(\frac{a}{R}\right)^2\right] / \left[0.58 \left(\frac{a}{R}\right)^2\right] \\ &\approx 0.43, \quad \tau = -1, \end{aligned} \quad (53)$$

which corresponds to the angle $\varphi \approx 25.5^\circ$.

The existence of transmissions associated with valley quantum numbers raised the lovely discussion on exploiting of the valley degree of freedom for development carbon-based electronics named graphene valleytronics [31]. Valley polarization, valley inversion [32], and valley-contrasting spatial confinement [33] of massless Dirac fermions were demonstrated experimentally in strained graphene under inhomogeneous pseudomagnetic fields and tunable real magnetic fields.

The results for transmission at $N \gg 1$ and $\varepsilon > E$ (see Figs. 3 and 5) indicate that propagating modes with the wave vector $k \in [0, k_F]$ lie in the K valley, whereas modes with the wave vector $k \in [0, -k_F]$ lie in the K' valley. At $\varepsilon < E$ we have the opposite situation. Therefore, for the sake of discussion we consider the most interesting case $\varepsilon > E$. With the aid of Eqs. (37), (38), and (40) the valley polarization of

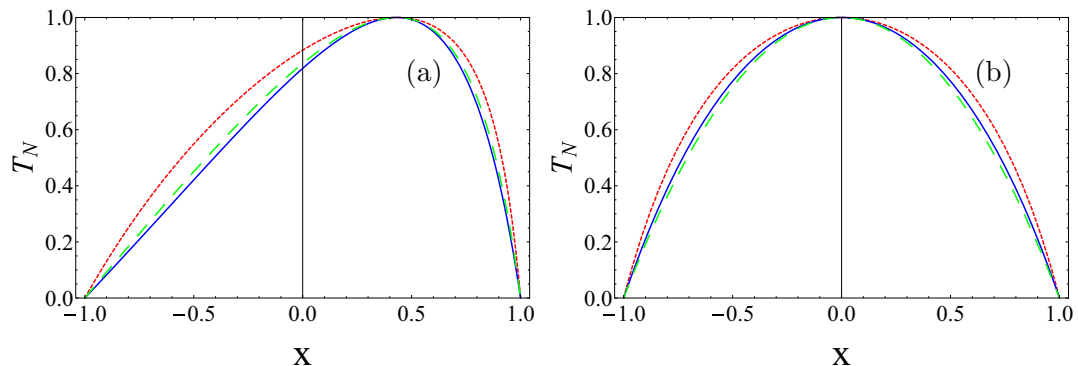


FIG. 7. Transmission probabilities T_N as a function of $x = k_y/k_F$ for the K' valley. The energy of the incoming electrons is $E = 1.001\varepsilon$, $L_1 = 10a$, $R = 18 \text{ \AA}$, and $\phi = \pi$; (a) armchair surface; (b) zigzag surface. The number of elements of the superlattice is similar to Fig. 3.

the transmitted current is quantified by

$$P_N^\tau = \frac{\int_0^{k_F} T_N^\tau(k_y, \tau\xi) \frac{dk_y}{2\pi/W} - \int_{-k_F}^0 T_N^\tau(k_y, \tau\xi) \frac{dk_y}{2\pi/W}}{\int_{-k_F}^{k_F} T_N^\tau(k_y, \tau\xi) \frac{dk_y}{2\pi/W}}, \quad (54)$$

where $\xi = |\Delta k_y|$, and the valley dependent Δk_y is defined by Eqs. (43) and (45); $\tau = (-/+)$ corresponds to K/K' valleys, respectively. Taking into account the results of calculations for the transmission probability (see Fig. 3), we obtain $P_N^K = P_N^{K'} = 0$ for the superlattice with zigzag edge termination for the both valleys. It is notable, that the conductivity is decreasing with the increase of the number of N elements, focusing between $\varphi \leq |20^\circ|$, being symmetric for the superlattice with zigzag edge termination. For superlattice with armchair edge termination, the polarization is $P \in [-1, 1]$, with $P = 1$ if the transmitted current lies fully in the K valley and $P = -1$ if it lies fully in the K' valley (see Fig. 5). In this case the conductivity decreases with the increase of the number of N elements of the superlattice.

IV. SUMMARY

Based on the fact of the different type of hybridization of carbon atom orbitals in the flat and the corrugated graphene pieces, we developed the model that simulates n - p junction by means of the superlattice and describes the valley focusing effect. In the approximation of the effective mass Hamiltonian, the curvature dependence of the π orbitals yields the variation of the local chemical potential. This fact corresponds to the effective electric field that depends on the electron localization. The variation of the graphene curvature affects the transfer integrals as well, that, together with the hybridization, provides the necessary conditions for the implementation of the valley focusing effect. It is notable that the modification of the transfer integrals becomes important in the corrugated graphene sheet with the armchair surface, while it is negligible in the case of the corrugated sheet with the zigzag surface.

Our analysis of the superlattice system that consists of the periodically repeated flat and ripple pieces demonstrates the strong selectivity effect of transmitted electron trajectories with the increase of number N (elements of the superlattice). This effect becomes essential for incident electrons, moving in the energy interval $0 < E < \varepsilon$, where ε is the energy difference between the π orbitals in the curved and flat graphene sheet. The ballistic electron transmission depends on the radius of the ripple, on the length of the arc of the ripple, and on the width of the flat region between ripples. It is remarkable, however, that in a multirippled graphene structure the maximum of the transmission for the both valleys is reached at different angles that are characteristic constants: $\varphi = 0^\circ$ for the structure with zigzag edge termination, and $|\varphi| \approx 25.5^\circ$ for the one with armchair termination. The superlattice, described in the paper, enables to one to control the filtering effect without any additional electrical or magnetic sources. The larger the number of elements N , the stronger is the selectivity. At $N \gg 1$, only for the direction perpendicular to the surface of the \mathcal{S} subsystem, there is almost the ideal transmission, while for the other angles ($k_y \neq 0$) there is the strong reflection for the superlattice with zigzag edge termination. In the superlattice with armchair edge termination, similar

filtering takes place at the supercollimation angle $|\varphi| \approx 25.5^\circ$. This phenomenon is due to the Klein tunneling that is grown in our system by virtue of controlled graphene surface curvature.

ACKNOWLEDGMENTS

M. Pudlak acknowledges the financial support by Slovak Grant Agency for Science VEGA under Grant No. VEGA 2/0076/23.

APPENDIX : HYBRIDIZATION IN A CURVED GRAPHENE

Let us compare the hybridization of π and σ orbitals in the flat and curved graphene systems. We consider the Hamiltonian for the K point (a similar approach can be applied for K' point). It depends on two operators $\hat{k}_x = -i\frac{\partial}{\partial x}$, $\hat{k}_y = -i\frac{\partial}{\partial y}$, and yields the equation for the envelope function of the flat graphene in the effective mass approximation (e.g., [34]):

$$\begin{pmatrix} \varepsilon_{2p} & \gamma(\hat{k}_x - i\hat{k}_y) \\ \gamma(\hat{k}_x + i\hat{k}_y) & \varepsilon_{2p} \end{pmatrix} \begin{pmatrix} F_A^K \\ F_B^K \end{pmatrix} = E \begin{pmatrix} F_A^K \\ F_B^K \end{pmatrix}. \quad (A1)$$

Here, the parameter $\gamma = \sqrt{3}\gamma_0 a/2$ depends on the length of the primitive translation vector $a = \sqrt{3}d \simeq 2.46 \text{ \AA}$ with d being the distance between atoms in the unit cell, and it is assumed that $\gamma_0 \approx 3 \text{ eV}$. The energy $\varepsilon_{2p} = \langle 2p_z | H'' | 2p_z \rangle$ is the energy of $2p_z$ orbitals of carbon atoms in the flat graphene, directed perpendicular to the graphene surface; H'' is the tight-binding Hamiltonian of the graphene. The solution of Eq. (A1) determines the wave function

$$F(x, y) = e^{ik_x x} e^{ik_y y} \frac{1}{\sqrt{2}} \begin{pmatrix} s e^{-i\varphi} \\ 1 \end{pmatrix}, \quad (A2)$$

$$e^{-i\varphi} = (k_x - ik_y) / \sqrt{k_x^2 + k_y^2},$$

and the energy

$$E = \varepsilon_{2p} + s\gamma \sqrt{k_x^2 + k_y^2}. \quad (A3)$$

Here, the sign $s = -1(+1)$ is associated with the valence (conductance) band. In the flat graphene we have the following hybridization of π and σ orbitals:

$$|\pi\rangle = |2p_z\rangle, \quad (A4)$$

$$|\sigma_1\rangle = \frac{1}{\sqrt{3}}|2s\rangle + \sqrt{\frac{2}{3}}|2p_y\rangle, \quad (A5)$$

$$|\sigma_2\rangle = \frac{1}{\sqrt{3}}|2s\rangle + \sqrt{\frac{2}{3}} \left(\frac{\sqrt{3}}{2}|2p_x\rangle - \frac{1}{2}|2p_y\rangle \right), \quad (A6)$$

$$|\sigma_3\rangle = \frac{1}{\sqrt{3}}|2s\rangle - \sqrt{\frac{2}{3}} \left(\frac{\sqrt{3}}{2}|2p_x\rangle + \frac{1}{2}|2p_y\rangle \right). \quad (A7)$$

Let us discuss in detail the hybridization of σ and π orbitals in the graphene with nonzero curvature. The σ orbitals create the bonds between carbon atoms, while the π orbitals determine the electronic properties of the graphene. For the sake of illustration we consider a zigzag nanotube.

For the curved graphene (the arc, characterized by the radius R) we obtain the space coordinates of the three nearest-neighbor vectors $\vec{\tau}_i$ in the following form:

$$\vec{\tau}_1 = d(0, 1, 0), \quad (\text{A8})$$

$$\vec{\tau}_2 = d\left(\frac{\sqrt{3}}{2} \cos \vartheta, -\frac{1}{2}, -\frac{\sqrt{3}}{2} \sin \vartheta\right), \quad (\text{A9})$$

$$\vec{\tau}_3 = d\left(-\frac{\sqrt{3}}{2} \cos \vartheta, -\frac{1}{2}, -\frac{\sqrt{3}}{2} \sin \vartheta\right), \quad (\text{A10})$$

where $\sin \vartheta = a/4R$. At the limit $R \rightarrow \infty$, the vectors $\vec{\tau}_i$ transform to those of the flat graphene. Evidently, the σ_i orbitals are determined by the vectors $\vec{\tau}_i$. As a result, the σ_i and π orbitals can be expressed as follows:

$$|\pi\rangle = d_1|2s\rangle + d_2|2p_x\rangle + d_3|2p_y\rangle + d_4|2p_z\rangle, \quad (\text{A11})$$

$$|\sigma_1\rangle = c_1|2s\rangle + \sqrt{1 - c_1^2}|2p_y\rangle, \quad (\text{A12})$$

$$|\sigma_2\rangle = c_2|2s\rangle + \sqrt{1 - c_2^2}(|\chi_1\rangle - |\chi_2\rangle), \quad (\text{A13})$$

$$|\sigma_3\rangle = c_3|2s\rangle - \sqrt{1 - c_3^2}(|\chi_1\rangle + |\chi_2\rangle), \quad (\text{A14})$$

$$|\chi_1\rangle = \frac{\sqrt{3}}{2} \cos \vartheta |2p_x\rangle, \quad (\text{A15})$$

$$|\chi_2\rangle = \frac{1}{2}|2p_y\rangle - \frac{\sqrt{3}}{2} \sin \vartheta |2p_z\rangle. \quad (\text{A16})$$

With the aid of the orthonormality conditions $\langle\sigma_i|\sigma_j\rangle = \delta_{ij}$, $\langle\pi|\sigma_j\rangle = 0$, and $\langle\pi|\pi\rangle = 1$, we determine the parameters $\{c_k, d_i\}$ and obtain the following expressions for the π and σ orbitals in the lowest order of the ratio a/R :

$$|\pi\rangle \approx |2p_z\rangle + \frac{a}{2\sqrt{6}R}|2s\rangle + \frac{a}{4\sqrt{3}R}|2p_y\rangle, \quad (\text{A17})$$

$$|\sigma_1\rangle = \frac{1}{\sqrt{3}}|2s\rangle + \sqrt{\frac{2}{3}}|2p_y\rangle, \quad (\text{A18})$$

$$|\sigma_2\rangle = \frac{1}{\sqrt{3}}|2s\rangle + \sqrt{\frac{2}{3}}\left(\frac{\sqrt{3}}{2}|2p_x\rangle - |\chi_3\rangle\right), \quad (\text{A19})$$

$$|\sigma_3\rangle = \frac{1}{\sqrt{3}}|2s\rangle - \sqrt{\frac{2}{3}}\left(\frac{\sqrt{3}}{2}|2p_x\rangle + |\chi_3\rangle\right), \quad (\text{A20})$$

$$|\chi_3\rangle = \frac{1}{2}|2p_y\rangle + \frac{\sqrt{3}a}{8R}|2p_z\rangle. \quad (\text{A21})$$

The π orbitals are the same for the zigzag and armchair nanotubes in the lowest order of a/R . They are used to create the Bloch function in the tight-binding approximation. As a result, we obtain the following π orbital energy of the curved graphene surface of radius R

$$\begin{aligned} \varepsilon_\pi &= \langle\pi|H''|\pi\rangle = \langle 2p_z|H''|2p_z\rangle + \frac{1}{24}\left(\frac{a}{R}\right)^2 \langle 2s|H''|2s\rangle \\ &+ \frac{1}{48}\left(\frac{a}{R}\right)^2 \langle 2p_y|H''|2p_y\rangle = \varepsilon_{2p} + \alpha\left(\frac{a}{R}\right)^2, \end{aligned} \quad (\text{A22})$$

$$\alpha = \frac{1}{24}\langle s|H''|s\rangle + \frac{1}{48}\langle p_y|H''|p_y\rangle. \quad (\text{A23})$$

Note, that the orbitals $2p_{y,z}$, $2s$ are localized on the same carbon atom and contribute to the π orbital energy [31], while there is no such contribution from the nondiagonal matrix elements. As a result, we obtain that the energy of the curved graphene consists of the energy of the flat graphene ε_{2p} , and the energy of the $2s$, $2p_y$ orbitals brought about by the curvature.

Using the numerical values for the energies of the $|s\rangle$ and $|p_y\rangle$ orbitals of the carbon atom $\langle s|H''|s\rangle = -12\text{eV}$, $\langle p_y|H''|p_y\rangle = -4\text{eV}$ (e.g., [35]), we obtain for the parameter $\alpha \simeq -0.58\text{eV}$.

-
- [1] L. E. F. Foa Torres, S. Roche, J.-C. Charlier, *Introduction to Graphene-Based Nanomaterials: From Electronic Structure to Quantum Transport* (Cambridge University Press, New York, 2014).
- [2] M. I. Katsnelson, *Graphene: Carbon in Two Dimensions* (Cambridge University Press, New York, 2012).
- [3] T. Ando, Theory of electronic states and transport in carbon nanotubes, *J. Phys. Soc. Jpn.* **74**, 777 (2005).
- [4] V. V. Cheianov, V. I. Fal'ko, Selective transmission of Dirac electrons and ballistic magnetoresistance of $n - p$ junctions in graphene, *Phys. Rev. B* **74**, 041403(R) (2006).
- [5] V. V. Cheianov and V. I. Fal'ko, B. L. Altshuler, The focusing of electron flow and a Veselago lens in graphene $p - n$ junctions, *Science* **315**, 1252 (2007).
- [6] M. Katsnelson, A. Geim, Electron scattering on microscopic corrugations in graphene, *Phil. Trans. R. Soc. A.* **366**, 195 (2008).
- [7] F. Guinea, M. I. Katsnelson, M. A. H. Vozmediano, Midgap states and charge inhomogeneities in corrugated graphene, *Phys. Rev. B* **77**, 075422 (2008).
- [8] Z. Wu, F. Zhai, F. M. Peeters, H. Q. Xu, K. Chang, Valley-dependent Brewster angles and Goos-Hänchen effect in strained graphene, *Phys. Rev. Lett.* **106**, 176802 (2011).
- [9] A. Contreras-Astorga, V. Jakubský, A. Raya, On the propagation of Dirac fermions in graphene with strain-induced inhomogeneous Fermi velocity, *J. Phys.: Condens. Matter* **32**, 295301 (2020).
- [10] M. Vozmediano, M. Katsnelson, F. Guinea, Gauge fields in graphene, *Phys. Rep.* **496**, 109 (2010).
- [11] M. Pudlak, R. G. Nazmitdinov, Klein collimation by rippled graphene superlattice, *J. Phys.: Condens. Matter* **31**, 495301 (2019).
- [12] S. Kumar, D. M. Parks, Strain shielding from mechanically activated covalent bond formation during nanoindentation of graphene delays the onset of failure, *Nano Lett.* **15**, 1503 (2015).
- [13] J. A. Baimova, S. V. Dmitriev, K. Zhou, A. V. Savin, Unidirectional ripples in strained graphene nanoribbons with clamped edges at zero and finite temperatures, *Phys. Rev. B* **86**, 035427 (2012).

- [14] B. Liu, C. D. Reddy, J. Jiang, J. A. Baimova, S. V. Dmitriev, A. A. Nazarov, K. Zhou, Morphology and in-plane thermal conductivity of hybrid graphene sheets, *Appl. Phys. Lett.* **101**, 211909 (2012).
- [15] Y. Zhang, M. Heiranian, B. Janicek, Z. Budrikis, S. Zapperi, P. Y. Huang, H. T. Johnson, N. R. Aluru, J. W. Lyding, N. Mason, Strain modulation of graphene by nanoscale substrate curvatures: A molecular view, *Nano Lett.* **18**, 2098 (2018).
- [16] G. Zhang, Y.-W. Zhang, Strain effects on thermoelectric properties of two-dimensional materials, *Mech. Mater.* **91**, 382 (2015).
- [17] M. M. Alyobi, C. J. Barnett, P. Rees, R. J. Cobley, Modifying the electrical properties of graphene by reversible point-ripple formation, *Carbon* **143**, 762 (2019).
- [18] A. L. V. de Parga, F. Calleja, B. Borca, M. C. G. Passeggi, J. J. Hinarejos, F. Guinea, R. Miranda, Periodically rippled graphene: Growth and spatially resolved electronic structure, *Phys. Rev. Lett.* **100**, 056807 (2008).
- [19] D. Maccariello, A. Al Taleb, F. Calleja, A. L. V. de Parga, P. Perna, J. Camarero, E. Gnecco, D. Farías, R. Miranda, Observation of localized vibrational modes of graphene nanodomains by inelastic atom scattering, *Nano Lett.* **16**, 2 (2016).
- [20] A. Politano, G. Chiarello, Plasmon modes in graphene: status and prospect, *Nanoscale* **6**, 10927 (2014).
- [21] G.-X. Ni, Y. Zheng, S. Bae, H. R. Kim, A. Pachoud, Y. S. Kim, C.-L. Tan, D. Im, J.-H. Ahn, B. H. Hong, B. Özyilmaz, Quasi-periodic nanoripples in graphene grown by chemical vapor deposition and its impact on charge transport, *ACS Nano* **6**, 1158 (2012).
- [22] B. Vasić, A. Zurutuza, R. Gajić, Spatial variation of wear and electrical properties across wrinkles in chemical vapour deposition graphene, *Carbon* **102**, 304 (2016).
- [23] M. Pudlak, R. G. Nazmitdinov, Spin-dependent electron transmission across the corrugated graphene, *Phys. E* **118**, 113846 (2020).
- [24] J. Buša, M. Pudlak, R. Nazmitdinov, Rippled graphene as an ideal spin inverter, *Symmetry* **15**, 1593 (2023).
- [25] T. Ando, Spin-orbit interaction in carbon nanotubes, *J. Phys. Soc. Jpn.* **69**, 1757 (2000).
- [26] B. Huard, J. A. Sulpizio, N. Stander, K. Todd, B. Yang, and D. Goldhaber-Gordon, Transport measurements across a tunable potential barrier in graphene, *Phys. Rev. Lett.* **98**, 236803 (2007).
- [27] T. Low, S. Hong, J. Appenzeller, S. Datta, M. S. Lundstrom, Conductance asymmetry of graphene p-n junction, *IEEE Trans. Elec. Dev.* **56**, 1292 (2009).
- [28] J.-L. Zheng, F. Zhai, Valley filtering and valley-polarized collective modes in bulk graphene monolayers, *Chin. Phys. B* **33**, 017203 (2024).
- [29] T. Fujita, M. B. A. Jalil, S. G. Tan, S. Murakami, Gauge fields in spintronics, *J. App. Phys.* **110**, 121301 (2011).
- [30] P. E. Allain, J. N. Fuchs, Klein tunneling in graphene: optics with massless electrons, *Eur. Phys. J. B* **83**, 301 (2011).
- [31] A. Rycerz, J. Tworzydło, C. W. J. Beenakker, Valley filter and valley valve in graphene, *Nat. Phys.* **3**, 172 (2007).
- [32] S.-Y. Li, Y. Su, Y.-N. Ren, L. He, Valley polarization and inversion in strained graphene via pseudo-Landau levels, valley splitting of real Landau levels, and confined states, *Phys. Rev. Lett.* **124**, 106802 (2020).
- [33] Y.-N. Ren, Y.-C. Zhuang, Q.-F. Sun, L. He, Magnetic-field-tunable valley-contrasting pseudomagnetic confinement in graphene, *Phys. Rev. Lett.* **129**, 076802 (2022).
- [34] R. Saito, G. Dresselhaus, and M. S. Dresselhaus, *Physical Properties of Carbon Nanotubes* (London: Imperial College Press, London, 2003).
- [35] W. M. Lomer, The valence bands in two-dimensional graphite, *Proc. Roy. Soc. A* **227**, 330 (1955).